



OPEN

Highly efficient removal of thallium(I) by facilely fabricated amorphous titanium dioxide from water and wastewater

Gaosheng Zhang^{1✉}, Jinglin Luo^{1,3}, Hanlin Cao⁴, Shengping Hu¹, Huosheng Li¹, Zhijing Wu¹, Yuan Xie⁵ & Xiangping Li^{2✉}

In this study, amorphous hydrous titanium dioxide was synthesized by a facile precipitation method at room temperature, aiming to effectively remove thallium(I) from water. The titanium dioxide prepared using ammonia as precipitant (TiO₂^I) is more effective for thallium(I) uptake than the one synthesized with sodium hydroxide (TiO₂^{II}). The TiO₂ obtained particles are amorphous, aggregates of many nanoparticles and irregular in shape. The thallium(I) uptake increases with the rise of solution pH value. Under neutral pH conditions, the maximal thallium(I) adsorption capacities of TiO₂^I and TiO₂^{II} are 302.6 and 230.3 mg/g, respectively, outperforming most of the reported adsorbents. The amorphous TiO₂ has high selectivity towards thallium(I) in the presence of multiple cations such as K⁺, Ca²⁺, Mg²⁺, Zn²⁺ and Ni²⁺. Moreover, the TiO₂^I is efficient in removing thallium(I) from real river water and mining wastewater. Additionally, the spent TiO₂^I can be regenerated using hydrochloric acid solution and reused. The Tl(I) adsorption is achieved via replacing the H⁺ in hydroxyl group on the surface of TiO₂ and forming inner-sphere surface complexes. Owing to its high efficiency, facile synthesis and environmental friendliness, the TiO₂^I has the potential to be used as an alternative adsorbent to remove Tl(I) from water.

As a non-essential heavy metal to living organisms, thallium (Tl) has attracted more and more attentions because of its high toxicity^{1–4}. Thallium occurs at very low levels in the natural aquatic environment^{1,2}. However, anthropogenic activities such as coal combustion, mining and processing of Tl-hosting minerals lead to the release of large amount of Tl into natural water bodies, which pose a great threat to aquatic biota and human health². To abate the health risk associated with exposure to thallium through drinking, stringent criteria for Tl concentration in water/wastewater have been established in many countries. For instance, in the United States, the USEPA has set 2 and 140 µg/L as the maximum Tl level in drinking water and wastewater discharged, respectively; in China, the limit of Tl in drinking water has been lowered to 0.1 µg/L and more stringent standard of 2 µg/L has been adopted as the discharge standard for industrial wastewater in some provinces^{3,4}.

In aquatic environment, thallium usually exists in two oxidation states: thallos (I) and thallic (III)³. Tl(I) is considered to be very mobile and thus difficult to remove, because it generally forms most stable compounds in natural waters^{1,5}. Therefore, in the thallium treatment domain most of the researches concerned Tl(I) removal. A variety of techniques including adsorption^{6,7}, oxidation/precipitation^{8–10}, ion exchange^{11,12}, solvent extraction^{13,14}, etc., have been used to treat Tl-containing water and wastewater. In comparison with other methods, adsorption has recently gained more and more attentions, due to the advantages of high efficiency, affordable cost, simple operation and little toxic sludge generation^{3,6}. Numerous adsorbents such as carbon materials^{15,16}, mineral materials^{17,18}, biomass materials¹⁹, Prussian blue and analogues^{20–22}, manganese oxides^{23–27} and titanium-based materials^{28–30}, have been employed to remove Tl(I) from water or wastewater.

¹Key Laboratory for Water Quality and Conservation of the Pearl River Delta, School of Environmental Science and Engineering, Ministry of Education, Guangzhou University, Guangzhou 510006, China. ²School of Chemistry and Chemical Engineering, Guangzhou University, Guangzhou 510006, China. ³Guangzhou Huake Environmental Protection Engineering Co., Ltd., Guangzhou 510655, China. ⁴Technical Centre for Soil, Agriculture and Rural Ecology and Environment, Ministry of Ecology and Environment, Beijing 100012, China. ⁵Guangdong Provincial Key Laboratory of Radioactive and Rare Resource Utilization, Shaoguan 512026, China. ✉email: gs Zhang@gzhu.edu.cn; lxping@gzhu.edu.cn

Titanium dioxide has been extensively investigated and used to remove heavy metal contaminants such as Cs(I), Cu(II), Pb(II), Cd(II), Ni(II), As(III), As(V), Cr(III), Cr(VI), U(VI) and Th(IV) from water or wastewater^{31–35}, owing to its nontoxicity, affordable cost, good chemical stability and high affinity for these ions. However, little work has been done on the removal of Tl(I) with titanium dioxide. For instance, Tl(I) adsorption on anatase TiO₂ (Degussa, P25) was studied by Kajitvichyanukul et al. and the maximal adsorption capacity was found to be only 6.3 mg/g under neutral pH conditions³⁶; Asadpour et al. investigated the Tl(I) adsorption on anatase TiO₂ nanoparticles synthesized via ultrasound method and found that its maximal adsorption capacity was 25 mg/g at pH 9.0³⁷; Zhang et al. evaluated the Tl(I) adsorption on commercial rutile nano-TiO₂ and determined that the maximum adsorption capacity was 51.2 mg/g at pH 7.0 ± 0.3³⁸. Evidently, these well-crystalline TiO₂ nanoparticles have relatively low Tl(I) adsorption capacity and are not feasible for Tl(I) removal. Therefore, it is vital and challenging to synthesize titanium dioxide with high-efficiency adsorption of Tl(I). The amorphous TiO₂ may be a feasible choice because it often possesses abundant active sites, which are responsible for Tl(I) adsorption. Recently, a poor crystalline TiO₂ had been prepared by a simple precipitation method in our laboratory. The as-synthesized TiO₂ demonstrated a high maximal Tl(I) adsorption capacity of 239 mg/g at pH 7.0 ± 0.1²⁹, which was remarkably superior to the well-crystalline TiO₂. In addition, it could be easily synthesized in large scale. This is very interesting and the amorphous TiO₂ might be a potential sorbent for effective Tl(I) removal because of its high performance, good chemical stability, cost-effectiveness, facile synthesis and environmental friendliness. However, to our best knowledge, the influence of precipitant used to prepare amorphous TiO₂ on Tl(I) adsorption has never been investigated. Additionally, adsorption behavior and mechanism of Tl(I) on the amorphous TiO₂ have never been systematically studied.

Hence, in this study, two different precipitants (NH₃·H₂O and NaOH) were used to synthesize the amorphous TiO₂ via a facile precipitation method at room temperature. The synthesized TiO₂ was characterized with a variety of techniques. The adsorption behaviors such as kinetics, isotherm, solution pH effect and coexisting cation influence were studied in details. Additionally, removal of thallium(I) from mining wastewater and natural river water was also evaluated. Moreover, a possible removal mechanism of thallium(I) was proposed.

Materials and methods

Materials. All chemicals such as Ti(SO₄)₂, NH₃·H₂O (30%), NaOH, NaNO₃, TlNO₃ and nano-TiO₂ (P25) were purchased from Sinopharm Chemical Reagent Co. Ltd (Shanghai, China) and were analytical grade and used without further purification. Tl(I) stock solution was prepared by dissolving TlNO₃ in deionized water. Prior to use, the working solution was freshly prepared by diluting Tl(I) stock solution to specified concentration with deionized water.

Preparation of titanium dioxide. Titanium dioxide was prepared by a simple chemical precipitation method at room temperature. Briefly, 7.2 g Ti(SO₄)₂ was dissolved in a 200 mL deionized water. Under vigorously stirring, 10% ammonia solution or 1 M NaOH solution was then dropwise added to the Ti(SO₄)₂ solution until the pH was raised to approximately 7.5. The white precipitates produced were washed for several times using deionized water, then filtrated and dried at 55 °C for 24 h. The obtained titanium dioxides were denoted as TiO₂^I (using NH₃·H₂O as precipitant) and TiO₂^{II} (using NaOH as precipitant), respectively. In addition, titanium dioxide was also prepared by forced hydrolysis of Ti(SO₄)₂ at 70 °C for 4 h, and the as-prepared sample was denoted as TiO₂^{III}.

Characterization. X-ray diffraction (XRD) analysis was performed on a PW3040/60 diffractometer (Philips Co., the Netherlands). The morphology of the synthesized and commercial TiO₂ was observed with a Sigma 500 field scanning electron microscope (FESEM) (Carl Zeiss, Germany) and transmission electron microscope (TEM) (JEM-1230, JEOL, Japan). X-ray photoelectron spectra (XPS) were collected on an AXIS Supra spectrometer (Shimadzu Co., Japan) with a monochromatic Al Kα X-ray source (1486.6 eV). The XPS results were collected in binding energy forms and fitted using a nonlinear least-squares curve-fitting program (XPSPEAK41 Software).

Tl(I) adsorption experiments. Batch tests were performed to estimate Tl(I) removal by the synthesized and commercial TiO₂. Briefly, 10 mg TiO₂ was added into 100 mL polyethylene bottles, which contain 50 mL Tl(I) solution with different concentrations. The solution pH was adjusted with 0.1 M NaOH and/or HNO₃. The bottles were then sealed and were shaken on an orbital oscillator at 180 rpm for 24 h. Afterwards, supernatant was collected and filtered through a 0.45 μm membrane. More detailed description of adsorption tests is shown in the Supplementary Material.

Tl(I) removal from real surface water and wastewater. To estimate the practicability of the synthesized TiO₂, Tl(I) removal from real wastewater and spiked surface water was studied by batch experiments. The surface water was collected from the Pearl River near to Guangzhou University, China and the mining wastewater was sampled from a mining area, Guizhou Province, China. The river water pH value was 7.56 and spiked Tl(I) concentration was 20 μg/L. More detailed parameters of water quality were listed in Table S1. The pH value of mining wastewater was 2.73 and Tl concentration was 4.9 μg/L. More detailed parameters of water quality were summarized in Table S2. For the spiked river water, defined amount of TiO₂^I (10 or 20 or 40 mg) was added into a 2000-mL beaker containing 1000 mL spiked Pearl River water. Afterwards, the solution was agitated by a magnetic stirrer at a speed of 200 rpm. 5 mL water sample was taken from the beaker at predetermined times. The samples were then filtered using a filter with 0.45-μm membrane. The residual Tl concentration was meas-

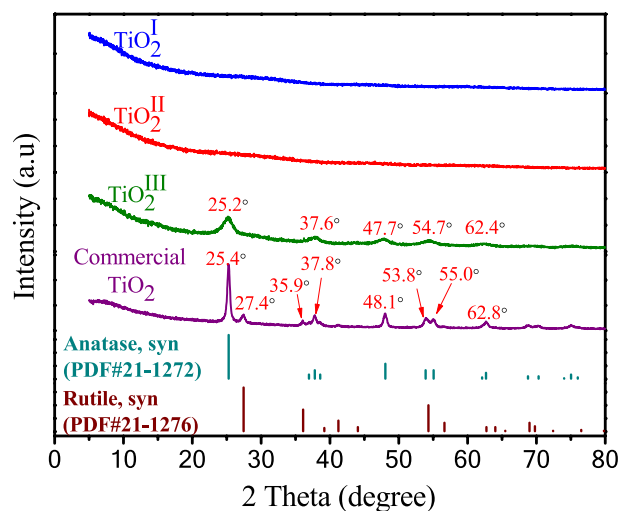


Figure 1. XRD patterns of synthesized and commercial TiO_2 .

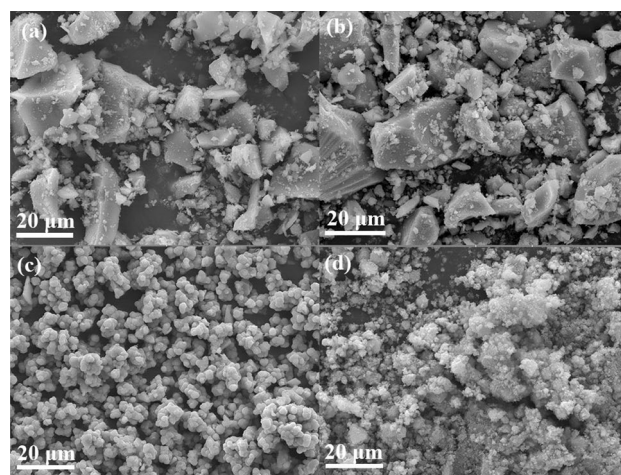


Figure 2. SEM images of TiO_2^{I} (a), TiO_2^{II} (b), $\text{TiO}_2^{\text{III}}$ (c) and commercial TiO_2 (d).

ured by an inductively coupled plasma mass spectrometry (ICP-MS). For mining wastewater, the test procedure was similar to the spiked river water.

Analytical methods. Before analysis, the aqueous samples collected were acidified with HNO_3 solution, and stored in glass bottles. Tl(I) concentration was determined by inductively coupled plasma mass spectrometry (ICP-OES, Avio 200, Perkin Elmer Co. USA). Trace level Tl was determined using an inductively coupled plasma mass spectrometry machine (ICP-MS, NexION 300, Perkin Elmer Co. USA).

Results and discussion

Characterization of TiO_2 . Figure 1 shows the X-ray diffraction patterns of synthesized and commercial titanium dioxides. For TiO_2^{I} and TiO_2^{II} , no obvious diffraction peaks can be observed, indicating that both of them are amorphous. Wang et al. had also synthesized amorphous TiO_2 and observed similar phenomenon³⁹. For $\text{TiO}_2^{\text{III}}$, five weak peaks appear at approximately 25.2, 37.6, 47.7, 54.7 and 62.4°, respectively, which are corresponding to the characteristic diffraction peaks of anatase (PDF#21-1272). This suggests that the anatase $\text{TiO}_2^{\text{III}}$ is not well-crystalline. For commercial TiO_2 , several strong peaks appear at 25.4°, 27.4°, 35.9°, 37.8°, 48.1°, 53.8°, 55.0° and 62.8°, respectively. The peaks at 25.4°, 37.8°, 48.1°, 53.8°, 55.0° and 62.8° coincide with those of anatase and peaks at 27.4 and 35.9° are in agreement with those of rutile, implying that the commercial TiO_2 contains both well-crystalline anatase and rutile phase. Figure 2 exhibits the SEM images of the synthesized and commercial titanium dioxides. As can be seen, both TiO_2^{I} and TiO_2^{II} are irregular in shape and constituted by many small particles, while the $\text{TiO}_2^{\text{III}}$ demonstrates a regular sphere-like shape with a particle size of 1–3 μm . The commercial TiO_2 particles are aggregates of smaller nanoparticles. TEM images of these four materials are demonstrated in Fig. 3. The TEM images of TiO_2^{I} and TiO_2^{II} further confirm that they are agglomerates of nanoparticles and

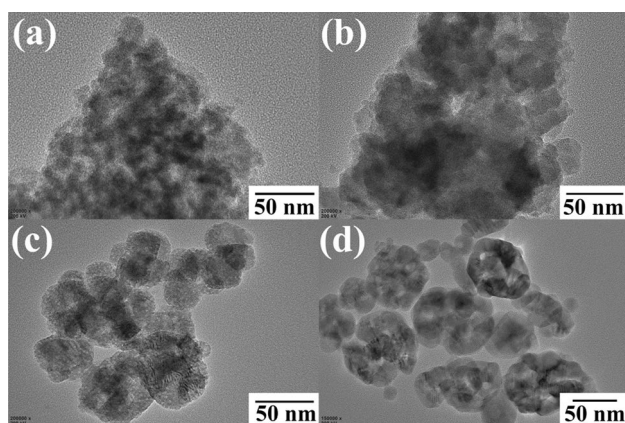


Figure 3. TEM images of TiO_2^{I} (a), TiO_2^{II} (b), $\text{TiO}_2^{\text{III}}$ (c) and commercial TiO_2 (d).

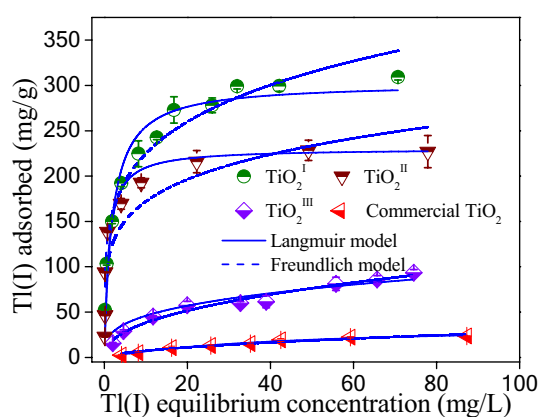


Figure 4. Adsorption isotherms of Tl(I) on the synthesized and commercial TiO_2 . Experiment conditions: Adsorbent dosage = 0.2 g/L; pH = 7.0 ± 0.1 and $T = 25 \pm 1$ °C.

amorphous. Relatively, the $\text{TiO}_2^{\text{III}}$ displays a polyhedron shape with certain crystallinity. The commercial TiO_2 presents well-crystalline nanoparticles with particle size of about 15–30 nm.

Adsorption isotherms. To evaluate the Tl(I) adsorption capacities of the synthesized and commercial titanium dioxides, the adsorption isotherm experiments were conducted at neutral circumstance. The results are illustrated in Fig. 4. Clearly, the adsorption capacities of synthesized titanium dioxides are far higher than that of the commercial one. Furthermore, the TiO_2 synthesized via chemical precipitation has much higher adsorption capacity than the one prepared by forced hydrolysis. The differences in the maximum adsorption capacity between them might be ascribed to their crystallinity. The amorphous TiO_2 may have more surface hydroxyl groups than well-crystalline TiO_2 , which are responsible for the Tl(I) adsorption. Interestingly, both TiO_2^{I} and TiO_2^{II} are rather efficient for Tl(I) removal, particularly for low concentration of Tl(I). In addition, it can be seen that the precipitant used to synthesize amorphous TiO_2 has great effect on Tl(I) adsorption. The TiO_2 obtained using $\text{NH}_3 \cdot \text{H}_2\text{O}$ as precipitant is much more effective for Tl(I) adsorption. However, extensive use of $\text{NH}_3 \cdot \text{H}_2\text{O}$ might lead to ammonia pollution. The experimental data were fitted by the Langmuir model (Eq. (S1)) and Freundlich model (Eq. (S2)). The fitting curves are demonstrated in Fig. 4 and the adsorption constants obtained from the isotherms are listed in Table 2. It can be observed that the Langmuir model is more suitable for describing the adsorption behavior, due to the higher regression coefficients (Table 1). This indicates that the Tl(I) adsorption on the TiO_2 follows a monolayer adsorption process, since the Langmuir model assumes that adsorption is limited to one monolayer. The maximal adsorption capacities of TiO_2^{I} , TiO_2^{II} , $\text{TiO}_2^{\text{III}}$ and commercial TiO_2 are 302.6, 230.3, 106.3 and 34.7 mg/g at pH 7.0, respectively. A comparison between the synthesized TiO_2 and adsorbents reported in literature for Tl(I) adsorption has been done (Table 2). Evidently, both TiO_2^{I} and TiO_2^{II} are more competitive than the majority of reported adsorbents, implying that amorphous TiO_2 is a promising alternative for Tl(I) removal from water. Therefore, investigation was focused on the TiO_2^{I} and TiO_2^{II} in the following sections.

Tl(I) adsorption kinetics. Figure 5 presents the adsorption kinetics data of Tl(I) on the TiO_2^{I} and TiO_2^{II} . A fast adsorption of Tl(I) was observed within the first 0.5 h. During this period, about 87.3 and 81.1% of equilib-

Adsorbent	Langmuir model			Freundlich model		
	q_{\max} (mg g ⁻¹)	k_L (L mg ⁻¹)	R^2	k_F (L g ⁻¹)	$1/n$	R^2
TiO ₂ ^I	302.6	0.528	0.951	139.7	0.208	0.949
TiO ₂ ^{II}	230.3	0.989	0.896	111.6	0.188	0.845
TiO ₂ ^{III}	104.3	0.059	0.933	22.4	0.312	0.921
Commercial TiO ₂	36.7	0.023	0.984	2.0	0.569	0.944

Table 1. Langmuir and Freundlich isotherms parameters for Tl(I) adsorption on the synthesized and commercial titanium dioxides at pH 7.0 ± 0.1.

Adsorbent	Tl equil. con. range (mg/L)	Dosage (g/L)	pH	Max. sorption capacity (mg/g)	References
TiO ₂ (Degussa, P25)	0–160	2.0	7.0	6.3	36
TiO ₂ nanoparticles	0–30	0.67	9.0	25	37
Nano-TiO ₂	0–12	–	7.0	51.2	38
TNTs	0–55	0.2	5.0	709.2	28
TNM-30	0–550	0.25	8.0	710.4	30
Titanium peroxide	0–70	0.2	7.0	412	29
MnO ₂	0–102	0.5	5.0	349	23
FeOOH-loaded MnO ₂	0–140	0.4	7.0	450	40
Fe–Mn binary oxide	0–400	0.5	10.0	236.4	41
MnO ₂ @pyrite cinder	0–40	0.5	12.0	320.1	42
Alginate-PB	0–400	1.0	4.0	103	22
MFBC	0–300	1.0	6.0	170	7
TFNPs	0–50	0.1	7.0	111.3	43
Biochar	0–300	2.0	6.5	178.4	44
ZnKFeCN@Fe ₃ O ₄ composite	0–160	0.6	7.0	120	45
Commercial TiO ₂	0–80	0.2	7.0	36.7	Present study
TiO ₂ ^{III}	0–80	0.2	7.0	104.3	Present study
TiO ₂ ^{II}	0–80	0.2	7.0	230.3	Present study
TiO ₂ ^I	0–80	0.2	7.0	302.6	Present study

Table 2. Comparison of Tl(I) maximal sorption capacities for different adsorbents.

rium Tl(I) adsorption capacity was achieved for TiO₂^I and TiO₂^{II}, respectively. Afterwards, the Tl(I) adsorption rate became slower and the equilibrium was established within about 4 h. Both the pseudo-first-order model (Eq. (S3)) and pseudo-second-order model (Eq. (S4)) were initially applied to stimulate the kinetic data. The fitting curves are depicted in Fig. 5 and constants obtained from these two models are provided in Table 3. In terms of R^2 , it has been found that the pseudo-second order model fits better the kinetic data than the pseudo-first order model, indicating that removal process of Tl(I) by the synthesized TiO₂ involves chemisorption.

Adsorption process is complicated and multi-step, involving bulk diffusion (adsorbate transport from the bulk solution to the outer surface of the liquid film), film diffusion (from the outer surface of the liquid film to the surface of the solid adsorbent), intraparticle diffusion (from the surface of the adsorbent to the interior pores), and adsorption on the surface actives of solid adsorbent^{46,47}. The pseudo-second order model is therefore limited in accuracy because it considers adsorption as a single, one-step binding process⁴⁸. Thus, intraparticle diffusion model (Eq. (S5)) was further used to describe the experimental data. The fitting results are shown in Fig. S1. For both TiO₂^I and TiO₂^{II}, the plot of q_t vs $t^{1/2}$ can be divided into two linear segments, indicating that Tl(I) adsorption contains multiple steps. The first linear section is corresponding to the fast adsorption stage, which is mainly controlled by film diffusion. The second linear section is a slow stage, which is governed by the diffusion of Tl(I) from the surface of adsorbent into the micropores.

Influences of pH and ionic strength on Tl(I) adsorption. The solution pH affects not only the species of metal ions but also the surface functional group on the adsorbents for metal ions capturing⁴⁹. Figure 6 demonstrates the influences of solution pH and ionic strength on Tl(I) adsorption. Evidently, Tl(I) adsorption on the TiO₂^I and TiO₂^{II} is strongly affected by the solution pH value, increasing gradually with its increase (2.0–9.0). And the optimal adsorption occurs under high alkaline circumstances. A similar trend was observed for the Tl(I) adsorption on titanium peroxide²⁹ and titanium iron magnetic adsorbent⁴³. In the tested pH range from 2.0 to 9.0, positively-charged Tl⁺ is the dominant species for Tl(I). Under acidic conditions, the surface of TiO₂ was favorably protonated and consequently positively charged, which resulted in strong electrostatic repulsion between Tl⁺ and the positively-charged surface and depression of Tl⁺ sorption. With the increase in solution pH

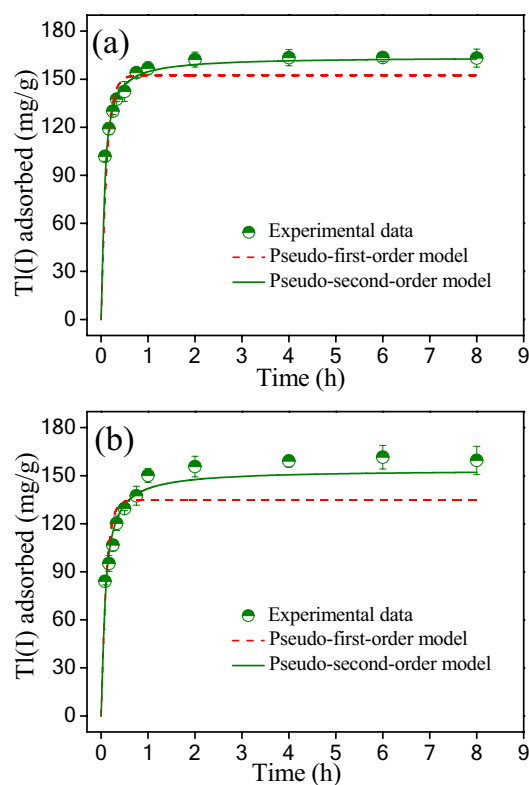


Figure 5. Kinetics of Tl(I) adsorption on TiO_2^{I} (a) and TiO_2^{II} (b). Experiment conditions: Initial Tl(I) concentration = 34.5 mg/L; adsorbent dosage = 0.2 g/L; pH = 7.0 ± 0.1 and $T = 25 \pm 1$ °C.

Adsorbent	Pseudo first order model			Pseudo second order model		
	q_e (mg g^{-1})	k_1 (h^{-1})	R^2	q_e (mg g^{-1})	K_2 ($\text{g mg}^{-1} \text{h}^{-1}$)	R^2
TiO_2^{I}	152.5	8.93	0.910	163.9	0.102	0.995
TiO_2^{II}	134.8	9.93	0.991	153.6	0.079	0.998

Table 3. Kinetic parameters for Tl(I) adsorption on the TiO_2^{I} and TiO_2^{II} fitted with the pseudo first order and pseudo second order models.

value, the TiO_2 surface became less positively-charged and turned to be negatively-charged, which was beneficial for the sorption of Tl^+ . Thus, the uptake of Tl^+ increased.

As can be seen in Fig. 6, the change in ionic strength (from 0.001 to 0.1 mM) did not greatly affect the adsorption of Tl(I) on both TiO_2^{I} and TiO_2^{II} . Adsorption of ions by formation of outer-sphere complexes is very sensitive to the ionic strength change and always decreases with an increase in ionic strength, since the background electrolyte ions can also form this kind of complex via electrostatic force. On the contrary, adsorption by formation of inner-sphere complexes is insensitive to the variation of ionic strength⁵⁰. Thus, it could be reasonably concluded that the Tl(I) was specifically adsorbed on the surface of TiO_2 by formation of inner-sphere complexes.

Influence of coexisting cations. Cations such as Ca^{2+} , Mg^{2+} and K^+ often exist in the surface water and groundwater^{51,52}. Moreover, heavy metal ions such as Zn^{2+} , Ni^{2+} and Cd^{2+} co-occur frequently with Tl^+ in the mining and industrial wastewaters. These present cations might compete for the adsorptive sites on the surface of TiO_2^{I} or TiO_2^{II} with Tl^+ . Therefore, the influence of these cations on Tl^+ adsorption was evaluated by batch tests at pH 4.5 ± 0.1 .

Figure 7 shows the experimental results. Interestingly, the coexisting K^+ , Ca^{2+} , Mg^{2+} , Zn^{2+} and Ni^{2+} do not greatly affect the Tl^+ adsorption and no great decrease is observed even though the concentration of present cations is as high as 10 mM. Awual et al. also found that the present K^+ did not greatly prevent the adsorption of Cs^+ (similar to Tl^+ in chemical properties) by crown ether based conjugate material⁵³. It is noteworthy that the coexisting Cd^{2+} inhibits Tl^+ adsorption. For the TiO_2^{I} , this negative effect is slight and the Tl^+ adsorption capacity still remains over 90% when the concentration of Cd^{2+} reaches up to 10 mM, being 100 times higher than that of initial Tl^+ . However, for the TiO_2^{II} , the negative influence is relatively remarkable and Tl(I) adsorption decreases

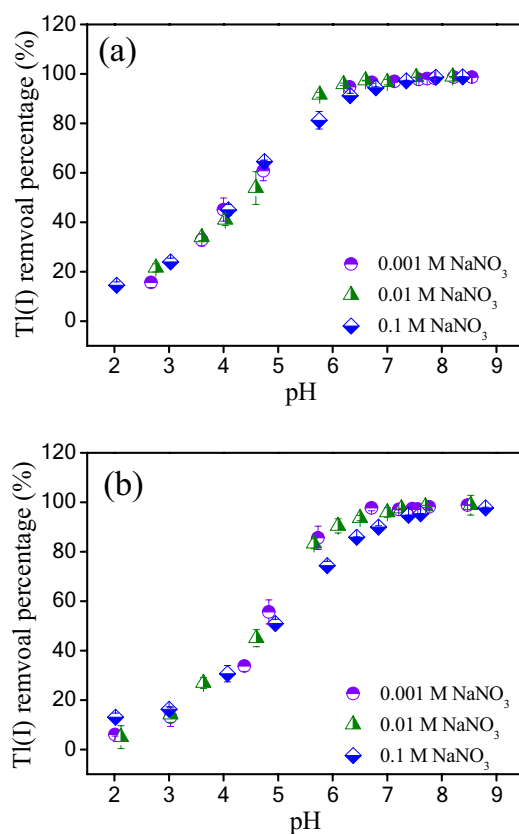


Figure 6. Effects of solution pH and ionic strength on Tl(I) adsorption by TiO₂^I (a) and TiO₂^{II} (b). Experimental conditions: Initial Tl(I) concentration: 30 mg/L; adsorbent dosage: 0.2 g/L; T: 25 ± 1 °C.

by about 29% as the concentration of Cd²⁺ increases from 0 to 10 mM. Relatively, both TiO₂^I and TiO₂^{II} has high selectivity towards Tl(I) in the presence of multiple cations.

From above, we can see that the adsorption behaviors of Tl(I) on TiO₂^I and TiO₂^{II} are very similar. Therefore, we only studied the applicability, regeneration and mechanism of Tl(I) removal by the TiO₂^I in the following sections.

Tl(I) removal from real surface water and wastewater. To evaluate the applicability of the TiO₂^I, kinetics of Tl(I) removal from the surface water (spiked Pearl River water) and mining wastewater were respectively investigated by batch tests. The results are shown in Fig. 8a,b, respectively. For the Pearl River water, when the dosage of TiO₂^I was 20 mg/L, the concentration of residual Tl(I) in the effluent was lowered to less 2 µg/L within 240 min (Fig. 8a). Tl(I) removal became more rapid as the dosage of TiO₂^I increased. When the dosage was 40 mg/L, the residual Tl(I) reduced to less 2 µg/L within 120 min and below 1 µg/L at 360 min. For mining wastewater, when the dosage was 25 mg/L, the Tl concentration in the effluent was below 2 µg/L after treatment for 210 min. As the dosage increased to 50 mg/L, the residual Tl decreased rapidly from 4.7 to less 2 µg/L within 30 min (Fig. 8b). These results suggest that the TiO₂^I is highly efficient for Tl(I) removal from the river water and real mining wastewater and has good applicability.

Regeneration and reusability of TiO₂^I. The regeneration and reusability of adsorbent is an important factor affecting its use in real water treatment⁵⁴. In order to assess the reusability of TiO₂^I, the Tl(I) desorption from spent adsorbent was investigated using 0.1 M HCl solution as desorbing agent and then the regenerated adsorbent was used in another adsorption–desorption cycle. Figure 9 illustrates the results of five consecutive adsorption/regeneration cycles. The cycle 0 is corresponding to the Tl(I) adsorption by the fresh TiO₂^I. As can be seen, the adsorption percentage of Tl(I) decreases with an increase in the number of cycles. After the first regeneration, the adsorption percentage of Tl(I) by the regenerated adsorbent reduces from 98.7 to 79.3%. This value is further lowered to 60.1% after the third regeneration and 45.3% after the fifth regeneration. Apparently, the reusability of TiO₂^I is moderate, which may be ascribed to the relatively strong affinity between Tl(I) and the TiO₂^I. These results suggest that the TiO₂^I could be regenerated but the times of reuse are limited.

XPS analysis before and after Tl(I) adsorption. In order to reveal the mechanism of Tl(I) adsorption by the TiO₂^I, XPS spectra of the TiO₂^I before and after Tl(I) uptake were determined and analyzed. Figure 10a

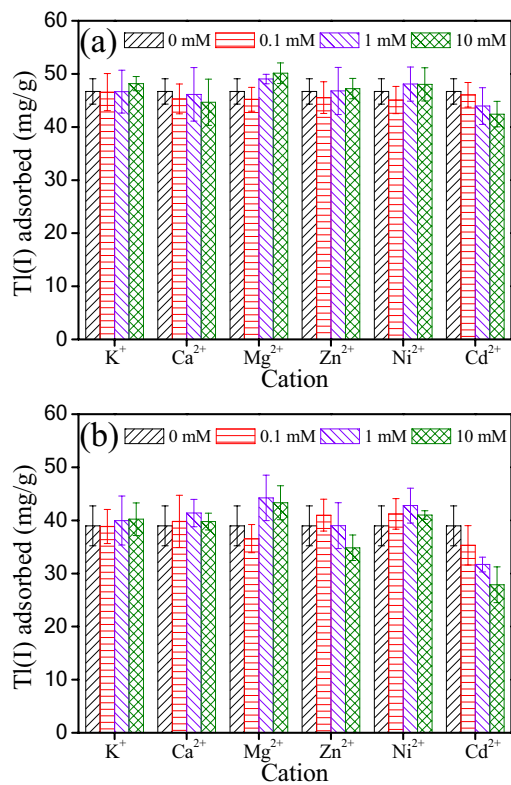


Figure 7. Influence of coexisting cations on Tl(I) adsorption by the TiO_2^I (a) and TiO_2^{II} (b). Experiment conditions: Tl(I) concentration = 18.5 mg/L; adsorbent dosage = 0.2 g/L; pH 4.5 ± 0.1 and $T = 25 \pm 1$ °C.

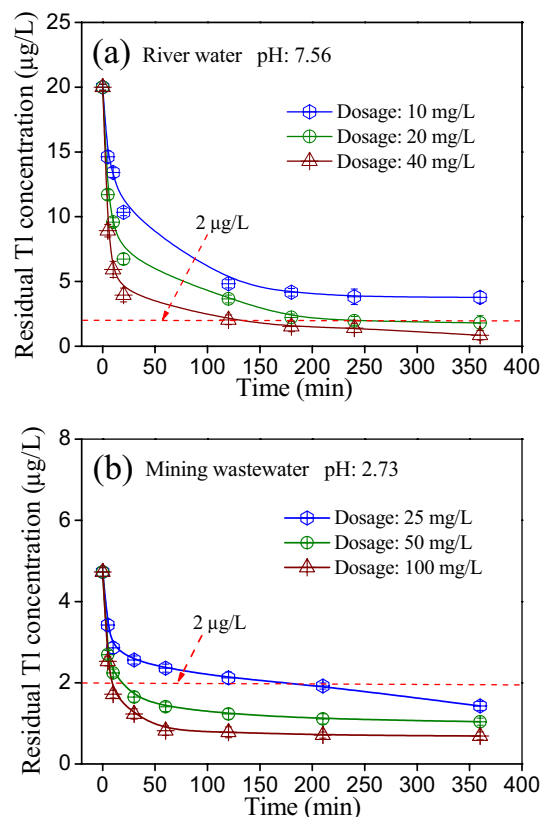


Figure 8. Kinetics of Tl(I) removal by TiO_2^I from the (a) spiked Pearl River water and (b) mining wastewater.

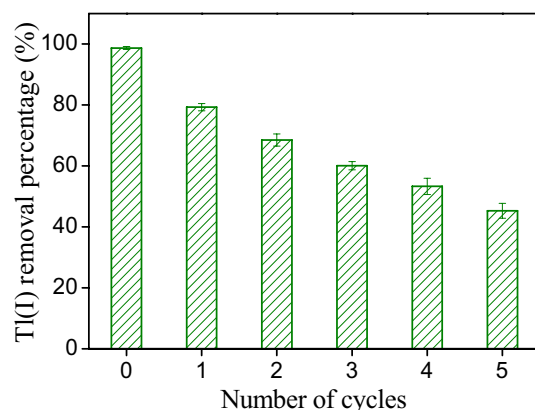


Figure 9. Variation of Tl(I) adsorption by the TiO_2^1 as a function of regeneration cycle.

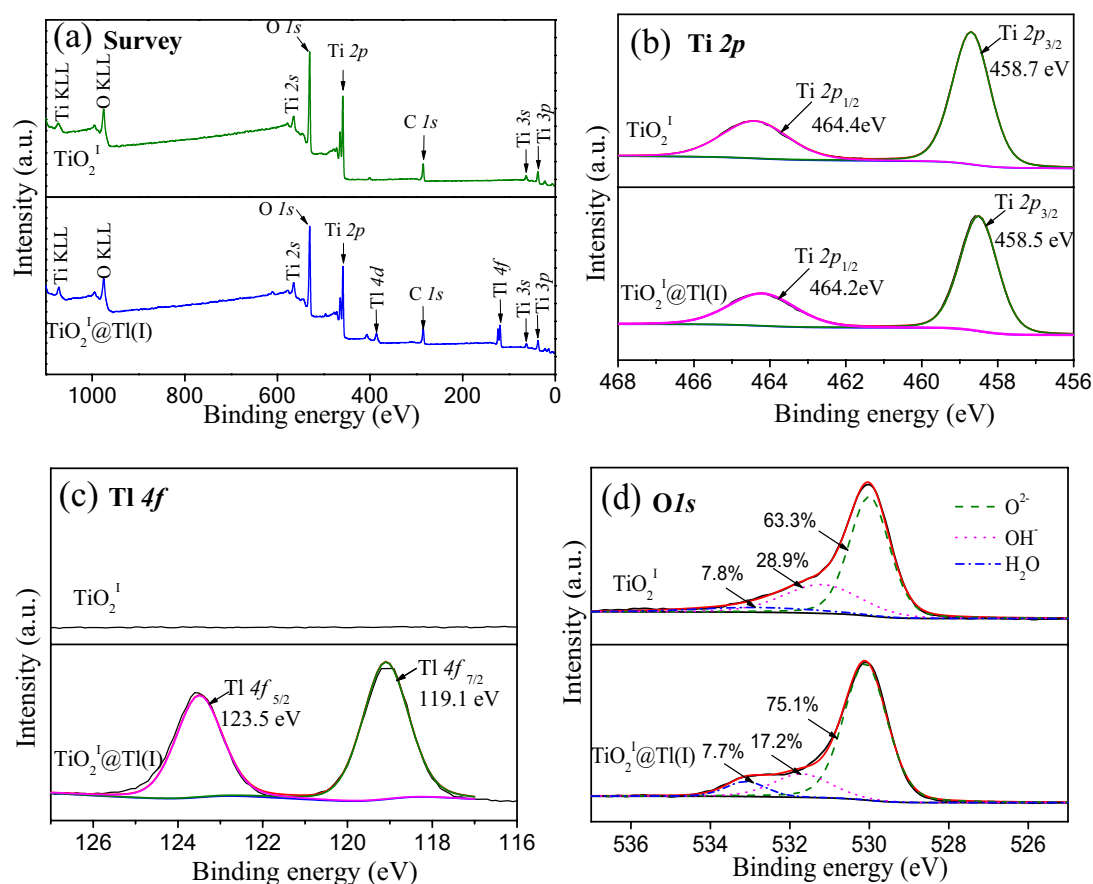


Figure 10. XPS spectra of TiO_2^1 before and after Tl(I) adsorption. (a) Survey spectra, (b) high-resolution Ti 2p spectra, (c) high-resolution Ti 4f spectra, (d) high-resolution O 1s spectra.

presents the survey spectra of the original and Tl(I)-sorbed TiO_2^1 . Characteristic Ti peaks including Ti 2p, Ti 2s, Ti 3p, Ti 3s and Ti KLL along with O peaks are observed in the spectra of the original TiO_2^1 . After reaction with Tl(I), two characteristic Tl peaks of Tl 4f and Tl 4d appear, suggesting that Tl(I) was adsorbed on the surface of TiO_2^1 . High resolution XPS spectra of Ti 2p, Ti 4f and O 1s of the pristine and Tl(I)-loaded TiO_2^1 are illustrated in Fig. 10b–d, respectively. The doublet peaks of Ti 2p_{3/2} and Ti 2p_{1/2} are located at 458.7 eV and 464.4 eV, respectively, indicating that the oxidation state of Ti in the TiO_2^1 is +4^{29,55,56}. These two peaks exhibit a slight shift (0.2 eV) to lower binding energy after Tl(I) sorption, which might be ascribed to the presence of strong interaction between TiO_2^1 and Tl(I). The two peaks of Tl 4f_{7/2} and Tl 4f_{5/2} are located at 119.1 eV and 123.5 eV, respectively, indicating that the oxidation state of Tl sorbed is +1²³. Obviously, no Tl(I) oxidation occurs during its adsorption by TiO_2^1 . The O 1s spectra can be divided into three peaks situated at 530.2, 531.7 and 533.1, cor-

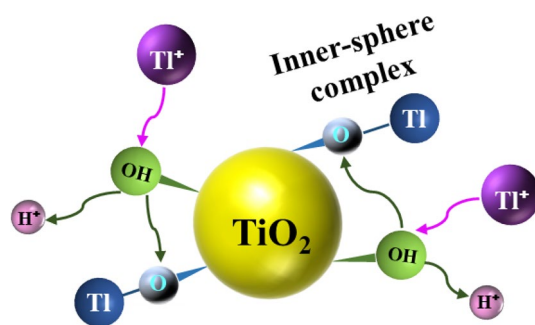


Figure 11. The proposed mechanism of Tl(I) adsorption on TiO_2 .

responding to lattice oxygen (O^{2-}), surface hydroxyl ($-\text{OH}$), and sorbed water (H_2O), respectively. For the virgin TiO_2^1 , the contents of O^{2-} , $-\text{OH}$ and H_2O are 63.3, 28.9 and 7.8%, respectively. After Tl(I) sorption, the content of H_2O showed no significant change, while the content of $-\text{OH}$ species decreased obviously from 28.9 to 17.2% and correspondingly, the content of O^{2-} increased from 63.3 to 75.1%. Obviously, the H^+ in $-\text{OH}$ group was replaced by the Tl(I) species during its removal.

From the above-mentioned analysis, a possible mechanism of Tl(I) removal by the TiO_2^1 was established and the schematic diagram was illustrated in Fig. 11. Firstly, the Tl^+ was transported to the surface of TiO_2^1 from bulk solution. Afterwards, the Tl^+ replaced the H^+ in $-\text{OH}$ group on the surface of TiO_2^1 and an inner-sphere surface complex ($\text{Ti}-\text{O}-\text{Tl}$) was formed. Meanwhile, the H^+ was released and entered into the bulk solution.

Conclusions

Hydrous titanium dioxide was facilely synthesized by precipitation method and forced hydrolysis method, respectively. The TiO_2 prepared at room temperature is amorphous and effective for Tl(I) adsorption, exhibiting high maximal adsorption capacities of 230.3–302.6 mg/g under neutral pH conditions. These values outperform the majority of reported adsorbents. The Tl(I) adsorption is strongly pH-dependent, increasing with an increase in solution pH value. The TiO_2 has high selectivity for Tl(I) adsorption and it can be used repeatedly, though the times of reuse are limited. The mechanism of Tl(I) removal is that the H^+ in $-\text{OH}$ on the surface of TiO_2 was replaced by Tl^+ and inner-sphere surface complex was formed. The synthesized TiO_2 has the potential to be used as an alternative adsorbent to remove Tl(I) from water, owing to its high efficiency, high stability, affordable cost, facile synthesis and environmental friendliness.

Received: 9 August 2021; Accepted: 8 December 2021

Published online: 07 January 2022

References

- Peter, A. L. J. & Viraraghavan, T. Thallium: a review of public health and environmental concerns. *Environ. Int.* **31**, 493–501 (2005).
- Xiao, T. F., Yang, F., Li, S. H., Zheng, B. S. & Ning, Z. P. Thallium pollution in China: A geo-environmental perspective. *Sci. Total Environ.* **421–422**, 51–58 (2012).
- Xu, H. Y. *et al.* Removal of thallium in water/wastewater: A review. *Water Res.* **165**, 114981 (2019).
- Liu, J. *et al.* Thallium pollution in China and removal technologies for waters: A review. *Environ. Int.* **126**, 771–790 (2019).
- Li, H. S. *et al.* Highly efficient removal of thallium(I) from wastewater via hypochlorite catalytic oxidation coupled with adsorption by hydrochar coated nickel ferrite composite. *J. Hazard. Mater.* **388**, 122016 (2020).
- Zhao, Z. *et al.* Adsorptive removal of trace thallium(I) from wastewater: A review and new perspectives. *J. Hazard. Mater.* **393**, 122378 (2020).
- Liu, J. *et al.* Highly efficient removal of thallium in wastewater by MnFe_2O_4 -biochar composite. *J. Hazard. Mater.* **401**, 123311 (2021).
- Davies, M., Figueroa, L., Wildeman, T. & Bucknam, C. The oxidative precipitation of thallium at alkaline pH for treatment of mining influenced water. *Mine Water Environ.* **35**, 77–85 (2016).
- Liu, Y. L. *et al.* Highly efficient removal of trace thallium from contaminated source waters with ferrate: Role of in situ formed ferric nanoparticle. *Water Res.* **124**, 149–157 (2017).
- Liu, Y. L. *et al.* Treatment of trace thallium in contaminated source waters by ferrate peroxidation and poly aluminium chloride coagulation. *Sep. Purif. Technol.* **227**, 115663 (2019).
- Sinyakova, M. A., Semenova, E. A. & Gamuletskaya, O. A. Ion exchange of copper(II), lanthanum(III), thallium(I), and mercury(II) on the “polysurmin” substance. *Russ. J. Gen. Chem.* **84**, 2516–2520 (2014).
- Li, H. S. *et al.* Simultaneous removal of thallium and chloride from a highly saline industrial wastewater using modified anion exchange resins. *J. Hazard. Mater.* **333**(Suppl C), 179–185 (2017).
- Zhang, X. Y., Yin, G. Y. & Hu, Z. G. Extraction and separation of gallium, indium and thallium with several carboxylic acids from chloride media. *Talanta* **59**, 905–912 (2003).
- Hassanien, M. M., Kenawy, I. M., Mostafa, M. R. & El-Dellay, H. Extraction of gallium, indium and thallium from aquatic media using amino silica gel modified by gallic acid. *Microchim. Acta* **172**, 137–145 (2011).
- Hanafi, A. Adsorption of cesium, thallium, strontium and cobalt radionuclides using activated carbon. *Asian J. Chem.* **1**, 292–300 (2010).
- Pu, Y. B. *et al.* Adsorption and desorption of thallium(I) on multiwalled carbon nanotubes. *Chem. Eng. J.* **219**, 403–410 (2013).
- Deng, H. M. *et al.* Adsorption of Tl(I) on Na-montmorillonite and kaolinite from aqueous solutions. *Environ. Earth Sci.* **75**, 752 (2016).

18. Wick, S., Baeyens, B., Fernandes, M. M. & Voegelin, A. Thallium adsorption onto illite. *Environ. Sci. Technol.* **52**, 571–580 (2018).
19. Birungi, Z. S. & Chirwa, E. M. N. The adsorption potential and recovery of thallium using green micro-algae from eutrophic water sources. *J. Hazard. Mater.* **299**, 67–77 (2015).
20. Rauws, A. & Canton, J. Adsorption of thallium ions by Prussian Blue. *Bull. Environ. Contam. Toxicol.* **15**, 335–336 (1976).
21. Sangvanich, T. *et al.* Selective capture of cesium and thallium from natural waters and simulated wastes with copper ferrocyanide functionalized mesoporous silica. *J. Hazard. Mater.* **182**, 225–231 (2010).
22. Vincent, T. *et al.* Thallium(I) sorption using Prussian blue immobilized in alginate capsules. *Carbohydr. Polym.* **99**, 517–526 (2014).
23. Wan, S. L. *et al.* Selective capture of thallium(I) ion from aqueous solutions by amorphous hydrous manganese dioxide. *Chem. Eng. J.* **239**, 200–206 (2014).
24. Pan, B. C. *et al.* Recyclable polymer-based nano-hydrous manganese dioxide for highly efficient Tl(I) removal from water. *Sci. China Chem.* **57**, 763–771 (2014).
25. Huangfu, X. L. *et al.* Adsorption and oxidation of thallium(I) by a nanosized manganese dioxide. *Water Air Soil Pollut.* **226**, 2272 (2015).
26. Li, K. K. *et al.* Synthesis of manganese dioxide with different morphologies for thallium removal from wastewater. *J. Environ. Manage.* **251**, 109563 (2019).
27. Wick, S., Pena, J. & Voegelin, A. Thallium sorption onto manganese oxides. *Environ. Sci. Technol.* **53**, 13168–13178 (2019).
28. Liu, W., Zhang, P., Borthwick, A. G. L., Chen, H. & Ni, J. R. Adsorption mechanisms of thallium(I) and thallium(III) by titanate nanotubes: Ion-exchange and co-precipitation. *J. Colloid Interface Sci.* **423**, 67–75 (2014).
29. Zhang, G. S., Fan, F., Li, X. P., Qi, J. Y. & Chen, Y. H. Superior adsorption of thallium(I) on titanium peroxide: Performance and mechanism. *Chem. Eng. J.* **331**, 471–479 (2018).
30. Wang, N. N. *et al.* Removal of thallium(I) from aqueous solutions using titanate nanomaterials: The performance and the influence of morphology. *Sci. Total Environ.* **717**, 137090 (2020).
31. Guan, X. H. *et al.* Application of titanium dioxide in arsenic removal from water: A review. *J. Hazard. Mater.* **215**, 1–16 (2012).
32. Liu, W. *et al.* Adsorption of Pb²⁺, Cd²⁺, Cu²⁺ and Cr³⁺ onto titanate nanotubes: Competition and effect of inorganic ions. *Sci. Total Environ.* **456**, 171–180 (2013).
33. Mahdavi, S., Jalali, M. & Afkhami, A. Heavy metals removal from aqueous solutions using TiO₂, MgO, and Al₂O₃ nanoparticles. *Chem. Eng. Commun.* **200**, 448–470 (2013).
34. Tsydenov, D. E., Shutilov, A. A., Zenkovets, G. A. & Vorontsov, A. V. Hydrous TiO₂ materials and their application for sorption of inorganic ions. *Chem. Eng. J.* **251**, 131–137 (2014).
35. Borai, E. H., Breky, M. M. E., Sayed, M. S. & Abo-Aly, M. M. Synthesis, characterization and application of titanium oxide nanocomposites for removal of radioactive cesium, cobalt and europium ions. *J. Colloid Interface Sci.* **450**, 17–25 (2015).
36. Kajitvichyanukul, P., Chenthamarakshan, C. R., Rajeshwar, K. & Qasim, S. R. Photocatalytic reactivity of thallium(I) species in aqueous suspensions of titania. *J. Electroanal. Chem.* **519**, 25–32 (2002).
37. Asadpour, S., Chamsaz, M., Entezari, M. H., Haron, M. J. & Ghows, N. On-line preconcentration of ultra-trace thallium(I) in water samples with titanium dioxide nanoparticles and determination by graphite furnace atomic absorption spectrometry. *Arab. J. Chem.* **9**, S1833–S1839 (2016).
38. Zhang, W. L. *et al.* Adsorption of thallium(I) on rutile nano-titanium dioxide and environmental implications. *PeerJ* **7**, e6820 (2019).
39. Wang, X. J. *et al.* Construction of amorphous TiO₂/BiOBr heterojunctions via facets coupling for enhanced photocatalytic activity. *J. Hazard. Mater.* **292**, 126–136 (2015).
40. Chen, M. Q. *et al.* FeOOH-loaded MnO₂ nano-composite: An efficient emergency material for thallium pollution incident. *J. Environ. Manage.* **192**, 31–38 (2017).
41. Li, H. S. *et al.* Removal of thallium from aqueous solutions using Fe-Mn binary oxides. *J. Hazard. Mater.* **338**, 296–305 (2017).
42. Li, H. S. *et al.* Efficient removal of thallium(I) from wastewater using flower-like manganese dioxide coated magnetic pyrite cinder. *Chem. Eng. J.* **353**, 867–877 (2018).
43. Tang, J. L. *et al.* Study on adsorption properties and mechanism of thallium onto titanium iron magnetic adsorbent. *Sci. Total Environ.* **694**, 133625 (2019).
44. Li, H. S. *et al.* Biochar derived from watermelon rinds as regenerable adsorbent for efficient removal of thallium(I) from wastewater. *Process Saf. Environ.* **127**, 257–266 (2019).
45. López, Y. C., Ortega, G. A., Martínez, M. A. & Reguera, E. Magnetic Prussian Blue derivative like absorbent cages for an efficient thallium removal. *J. Clean. Prod.* **283**, 124587 (2021).
46. Badruzzaman, M., Westerhoff, P. & Knappe, D. R. U. Intraparticle diffusion and adsorption of arsenate onto granular ferric hydroxide (GFH). *Water Res.* **38**, 4002–4012 (2004).
47. Pan, S. Y., Syu, W. J., Chang, T. K. & Lee, C. H. A multiple model approach for evaluating the performance of time-lapse capsules in trapping heavy metals from water bodies. *RSC Adv.* **10**, 16490–16501 (2020).
48. D'Arcy, M., Weiss, D., Bluck, M. & Vilar, R. Adsorption kinetics, capacity and mechanism of arsenate and phosphate on a bifunctional TiO₂-Fe₂O₃ bi-composite. *J. Colloid Interf. Sci.* **364**, 205–212 (2011).
49. Kubra, K. T. *et al.* Utilizing an alternative composite material for effective copper(II) ion capturing from wastewater. *J. Mol. Liq.* **336**, 116325 (2021).
50. McBride, M. B. A critique of diffuse double layer models applied to colloid and surface chemistry. *Clays Clay Miner.* **45**, 598–608 (1997).
51. Awual, M. R. A novel facial composite adsorbent for enhanced copper(II) detection and removal from wastewater. *Chem. Eng. J.* **266**, 368–375 (2015).
52. Awual, M. R., Hasan, M. M., Khaleque, M. A. & Sheikh, M. C. Treatment of copper(II) containing wastewater by a newly developed ligand based facial conjugate materials. *Chem. Eng. J.* **288**, 368–376 (2016).
53. Awual, M. R., Yaita, T., Kobayashi, T., Shiwaku, H. & Suzuki, S. Improving cesium removal to clean-up the contaminated water using modified conjugate material. *J. Environ. Chem. Eng.* **8**, 103684 (2020).
54. Awual, M. R. *et al.* Ligand based sustainable composite material for sensitive nickel(II) capturing in aqueous media. *J. Environ. Chem. Eng.* **8**, 103591 (2020).
55. Xiong, L. B., Li, J. L., Yang, B. & Yu, Y. Ti³⁺ in the surface of titanium dioxide: Generation, properties and photocatalytic application. *J. Nanomater.* **2012**, 1–13 (2012).
56. Xin, X. Y., Xu, T., Wang, L. & Wang, C. Y. Ti³⁺-self doped brookite TiO₂ single-crystalline nanosheets with high solar absorption and excellent photocatalytic CO₂ reduction. *Sci. Rep.* **6**, 23684 (2016).

Acknowledgements

The authors acknowledge the financial support from National Natural Science Foundation of China (No. 51678562) and the Research Fund Program of Guangdong Key Laboratory of Radioactive and Rare Resource Utilization (2018B030322009).

Author contributions

G.Z.: Conceptualization; Writing—Original draft preparation. J.L.: Investigation; Validation. H.C.: Investigation; Formal analysis. S.H.: Investigation. H.L.: Data Curation; Formal analysis. Z.W.: Investigation. Y.X.: Investigation. X.L.: Conceptualization, Writing—Reviewing and Editing.

Competing interests

The authors declare no competing interests.

Additional information

Supplementary Information The online version contains supplementary material available at <https://doi.org/10.1038/s41598-021-03985-3>.

Correspondence and requests for materials should be addressed to G.Z. or X.L.

Reprints and permissions information is available at www.nature.com/reprints.

Publisher's note Springer Nature remains neutral with regard to jurisdictional claims in published maps and institutional affiliations.



Open Access This article is licensed under a Creative Commons Attribution 4.0 International License, which permits use, sharing, adaptation, distribution and reproduction in any medium or format, as long as you give appropriate credit to the original author(s) and the source, provide a link to the Creative Commons licence, and indicate if changes were made. The images or other third party material in this article are included in the article's Creative Commons licence, unless indicated otherwise in a credit line to the material. If material is not included in the article's Creative Commons licence and your intended use is not permitted by statutory regulation or exceeds the permitted use, you will need to obtain permission directly from the copyright holder. To view a copy of this licence, visit <http://creativecommons.org/licenses/by/4.0/>.

© The Author(s) 2022